LUT University

Use of the quasi-static Johnson-Cook model in the failure assessment of tensile specimens with metallurgical constraints

Neuvonen Riku, Skriko Tuomas, Björk Timo

Please cite the publication as follows:

Use of the Quasi-Static Johnson-Cook Model in the Failure
Assessment of Tensile Specimens With Metallurgical Constraints
Riku Neuvonen, Tuomas Skriko, Timo Björk

31.3.2020

1   USE OF THE QUASI-STATIC JOHNSON-COOK MODEL IN THE FAILURE ASSESSMENT
2   OF TENSILE SPECIMENS WITH METALLURGICAL CONSTRAINTS

3   Riku Neuvonen [a], *, Tuomas Skriko [b] **, Timo Björk [a], ***

4   [a] Laboratory of Steel Structures, Lappeenranta-Lahti University of Technology LUT, Finland, PL20, 53851 Lappeenranta.
5   [b] Laboratory of Welding Technology, Lappeenranta-Lahti University of Technology LUT, Finland, PL20, 53851 Lappeenranta.
6   * Riku Neuvonen, riku.neuvonen@lut.fi
7   ** Tuomas Skriko, tuomas.skriko@lut.fi
8   *** Timo Björk, timo.bjork@lut.fi
9   Declarations of interest: none

10   **Abstract**

11   Direct quenching has recently been used to develop cost-effective novel high and ultra-high strength
12   steels. In weldments made of these steels, a distinct soft zone, which can lower the ultimate strength and
13   deformation capacity of the welded joint, can form in the heat affected zone of the joint. In order to accurately
14   estimate the static strength and deformation capacity of a welded steel structure fabricated from these steels, the
15   effect of this softening must be taken into account. In this study, the effect of the softened zone is explored based
16   on round tensile test specimens with metallurgical constraints using experiments and numerical calculations. The
17   applicability of the quasi-static part of the Johnson-Cook material model and failure model for fracture assessment
18   under given conditions was hereby examined. Firstly, the material parameters were determined for direct-
19   quenched armor steel and cold-formed structural steel using notched tensile test specimens and FE models
20   combined with an optimization routine. A good agreement was achieved between the tests and the results from
21   the FE models for the notched specimens. Specimens with metallurgical constraints were manufactured from the
22   materials using rotational friction welding, and the corresponding FE models were created using the material
23   parameters obtained from optimization. Two different fracture mechanisms were observed in the tensile tests
24   conducted for the specimens with metallurgical constraints, namely cup and cone fractures at the center of the
25   specimen and fractures near the weld interface. In the corresponding FE models, the fracture initiations were
26   observed in the same areas. A good agreement between the FE models and experimental tensile tests was thus
27   achieved in the case of the cup and cone fractures. However, the generated FE models underestimated the fracture
28   displacement in the specimens where the fracture occurred near the weld interface.
29
30   Keywords: ultra-high strength steel; material modeling; mechanical properties; welded joints; fracture behavior;
31   failure assessment

Nomenclature (symbols are defined in their order of appearance)

$\overline{\sigma}_{\text{flow}}$	von Mises flow stress	σ^*	ratio of pressure divided by effective stress
A	yield limit	p	hydrostatic pressure
B	hardening coefficient	σ_{eff}	effective stress
$\overline{\varepsilon}_{\text{p}}$	equivalent plastic strain	L	Lode parameter
n	hardening exponent	$\sigma_1,\ \sigma_2,\ \sigma_3$	first, second and third principal stress component
C	viscous effect	D_1,D_2,D_3,D_4,D_5	fracture strain constants
$\dot{\varepsilon}^*$	dimensionless plastic strain rate	$R_{\text{p0.2}}$	0.2 % offset yield strength
T^*	homologous temperature	f_{u}	ultimate tensile strength
m	thermal sensitivity	A_t	elongation at fracture
$\dot{\varepsilon}$	effective plastic strain rate	A_5	elongation at fracture
$\dot{\varepsilon}_{\text{ref}}$	reference strain rate	D_i	instantaneous minimum diameter of a specimen
T	deformation temperature	M	tensile strength mismatch
T_{ref}	reference temperature	D_a	original minimum diameter of a specimen
T_m	melting temperature	L_{FL}	weld interface distance
D	damage parameter	δ_{30}	displacement at fracture, gauge length 30 mm
$\overline{\varepsilon}_f$	equivalent fracture strain		

**Use of the Quasi-Static Johnson-Cook Model in the Failure
Assessment of Tensile Specimens With Metallurgical Constraints**
Riku Neuvonen, Tuomas Skriko, Timo Björk

31.3.2020

1 **1. Introduction**

2 In recent years, novel high and ultra-high strength structural and armor steels have been produced using
3 direct quenching (DQ). In the DQ process, the quenching is performed immediately after the thermomechanical
4 rolling of the plate. After quenching, the plates can be tempered if necessary [1]. According to [2, 3], the DQ
5 process offers a cost-effective way to produce low-carbon martensitic and/or bainitic steel plates. Studies
6 conducted by Chang [4], Meysami et al. [5] and Muckelroy, Findley and Bodnar [2] indicate that the mechanical
7 properties of steels produced using the DQ process differ from those of steels produced using conventional
8 quenching and tempering.

9 The fabrication of steel structures often requires joining steel parts together. One important joining
10 method is welding, which alters the mechanical properties of the steel due to the chemical and metallurgical
11 changes caused by the thermal cycle of the welding process. The susceptibility to these changes depends on the
12 chemical composition and metallurgical structure of the steel.

13 According to Porter [6], DQ steels are susceptible to heat affected zone (HAZ) softening due to the low
14 carbon content. However, Amraei et al. [7] showed that by decreasing the width to plate thickness ratio of the
15 softened HAZ in S960 DQ steels, the strength and ductility of the joint can be increased due to the boundary
16 conditions generated by the higher strength of the material around the soft zone. Ran et al. [8] observed the same
17 behavior in various steel grades, but they also noted that ductility decreases due to a tensile strength mismatch
18 generated by the softened zone. Sun et al. [9] and Rodrigues et al. [10] noticed that in addition to the width of the
19 softened zone, the mismatch ratio and the hardening parameters of the adjacent materials have an effect on the
20 degree of the strengthening of the boundary conditions generated by the metallurgical constraints. In addition,
21 Björk et al. [11] demonstrated that in certain welds with a softened zone, a fracture can occur near the weld toe or
22 at the fusion line. This phenomenon can reduce the load-carrying and deformation capacity of the joints. On the
23 other hand, Skriko [12] showed that by using proper welding procedures and parameters, including heat input,
24 working temperature and groove preparation, a good performance quality of weldments made of S960 DQ steel
25 can be achieved despite the softening susceptibility of the steel.

26 In general, armor steels have high carbon equivalent values (CEV), making them susceptible to
27 hydrogen cracking [13]. In order to minimize cracking, proper heat input and suitable, preferably low strength,
28 filler metal is usually recommended by steel manufacturers. In addition to the mismatch, direct quenched armor
29 steels (DQA) are prone to HAZ softening. Thus, research into the metallurgical constraints is relevant for DQA
30 steels in order to obtain information on defining suitable workshop methods for this type of steel.

31 As was noted above, in order to investigate the effects of metallurgical constraints, reliable material
32 models must be applied. In this study, the material model developed by Johnson and Cook [14, 15] is applied
33 because it has been successfully used in several studies related to the stress-strain behavior and ductile fracture of
34 conventional armor steels [16, 17, 18, 19, 20, 21, 22].

35 Welding, especially multipass welding, generates complex microstructural changes in the HAZ [23],
36 and identifying and characterizing the material parameters for all the microstructurally different zones would
37 require substantial effort. On the other hand, using a simplified representation of the zones would require more or
38 less arbitrary assumptions about the importance of each zone to the overall behavior and properties of the
39 weldment. In order to minimize these issues, rotational friction welding was used in this study to manufacture
40 tensile test specimens with metallurgical constraints with clearly definable zones. This procedure enabled the
41 characterization of material parameters for the Johnson-Cook model using separate tensile test specimens. The
42 material parameters were obtained using an optimization routine and were verified by comparing the FE results
43 with results from the tensile specimens that were not used in the parameter identification. Verified and predefined
44 material models were applied in order to investigate the applicability of the Johnson-Cook model to assess the
45 fractures occurring in the softened zone restricted by boundary conditions caused by the metallurgical constraints.

46 **2. Theoretical Background**

47 The constitutive and fracture model developed by Johnson and Cook has been used successfully in
48 many studies on the behavior of steels [16, 17, 18, 19, 20, 21, 22]. Some researchers have subsequently modified
49 this model, such as Børvik et al. [24], whose modified model has, in turn, also been used by Banerjee et al. [25]
50 with good results. The Johnson-Cook constitutive model defines the von Mises equivalent flow stress using the
51 equation

$$\bar{\sigma}_{flow} = \left[A + B\bar{\varepsilon}_p^n\right]\left[1 + C\ln\dot{\varepsilon}^*\right]\left[1 - (T^*)^m\right] \tag{1}$$

1   The first bracket of the equation describes the hardening behavior, the second bracket takes the strain rate effect
2   into account, and the third bracket considers the temperature sensitivity. In the equation, A is the yield strength of
3   the material, B is the strain hardening constant, n is the strain hardening coefficient, C is the strengthening
4   coefficient of strain rate, m is the thermal softening coefficient and $\bar{\varepsilon}_p$ is the equivalent plastic strain. Dimensionless
5   plastic strain rate $\dot{\varepsilon}^*$ and homologous temperature T^* are defined by following equations, respectively

$$\dot{\varepsilon}^* = \frac{\dot{\varepsilon}}{\dot{\varepsilon}_{\text{ref}}} \tag{2}$$

$$T^* = \frac{T - T_{\text{ref}}}{T_{\text{m}} - T_{\text{ref}}} \tag{3}$$

6   where $\dot{\varepsilon}$ is the effective plastic strain rate, T is the deformation temperature and T_{m} is the melting temperature of
7   the material. $\dot{\varepsilon}_{\text{ref}}$ and T_{ref} are the reference strain rate and the reference deformation temperature, respectively. In
8   the fracture model described by Johnson and Cook, damage to the material is defined using the equation

$$D = \sum \frac{\Delta\bar{\varepsilon}_p}{\bar{\varepsilon}_f(\sigma^*, \dot{\varepsilon}^*, T^*)} \tag{4}$$

9   where $\bar{\varepsilon}_f$ is the equivalent fracture strain, which is defined

$$\bar{\varepsilon}_f = \left[D_1 + D_2 \exp D_3 \sigma^*\right]\left[1 + D_4 \ln\dot{\varepsilon}^*\right]\left[1 - D_5 T^*\right] \tag{5}$$

10   where D_1, D_2, D_3 constants describe the effect of stress triaxiality on effective plastic strain at fracture. D_4 and D_5
11   represent the material fracture sensitivity to strain rate and temperature. In this model, a fracture occurs when
12    $D=1$. In the model, σ^* is defined by following equation

$$\sigma^* = \frac{p}{\sigma_{\text{eff}}} \tag{6}$$

13   where p is the pressure and σ_{eff} is the effective stress.

14   In this paper, the main focus is on the quasi-static behavior of round specimens with different
15   metallurgical constraints at room temperature with the aim of determining the applicability of the Johnson-Cook
16   model to predict failure under the given conditions. In the quasi-static regime, the strain rate and temperature have
17   a minuscule effect on constitutive and fracture behavior [26]. Thus, the parameters governing the strain rate and
18   temperature behavior are not covered in this paper, even though these parameters are usually important in
19   applications related to armor steels, e.g. ballistic analyses.

20   In recent years, several researchers, such as [27, 28, 29], have noticed that in addition to the stress
21   triaxiality, the Lode parameter L also determines the amount of effective plastic strain that a material can
22   withstand. The Lode parameter can be defined by the following equation

$$-1 \le -\frac{2\sigma_2 - \sigma_1 - \sigma_3}{\sigma_3 - \sigma_1} \le 1 \tag{7}$$

23   where σ_1, σ_2, σ_3 are the first, second and third principal stress components, respectively. Important special cases
24   are when Lode parameter is equal to -1, 0 and 1, which corresponds to the conditions of axisymmetric uniaxial
25   compression, plane strain and axisymmetric uniaxial tension, respectively. The fracture model described in
26   equation (4) does not take into account the effect of Lode parameter. In this study, the effect of Lode parameter
27   was not studied in detail because the chosen material model could not take into account the effect. However, as
28   can been seen in the Results section, the metallurgical constraint generates a stress state where the Lode parameter
29   is not constant across the specimen.

30   A common method for the analytical interpretation of tensile tests is to use the formulas developed by
31   Bridgman [30]. Alves and Jones [31] and Bao [32] studied the accuracy of Bridgman's equations using FE
32   calculations, and they found that the equivalent strain at the minimum cross-section after necking and in notched
33   specimens is not constant. In the center of the specimen, Bridgman's solution overestimated the value of the
34   equivalent strain and underestimated it on the surface of the specimen, especially when the notch radius is small.
35   Alves and Jones [31] concluded that the difference between the numerical solution and Bridgman's solution is
36   negligible when the notch radius is large.

37   Bao [32] also reported that equivalent strain is not constant in the minimum cross-section. The study
38   compared the stress values obtained using Bridgman's equations and the FE calculations. According to Bao's [32]
39   results, there is a 30-50 % difference in the stress values between the numerical solution and Bridgman's solution.

40   In addition, Alves and Jones [31] also studied the effect of strain hardening on the stress and strain state
41   of a notched tensile specimen using numerical calculations. They noticed that the development of the stress

Use of the Quasi-Static Johnson-Cook Model in the Failure
Assessment of Tensile Specimens With Metallurgical Constraints
Riku Neuvonen, Tuomas Skriko, Timo Björk

31.3.2020

1 triaxiality at the center of the specimen depends on the strain hardening behavior of the material. Bridgman does
2 not take this effect into account in his equations.
3   Because of these reported issues, analytical calculations to determine the material parameters were not
4 used in this study. Instead, the identification was based on measured values of the force, displacement and cross-
5 section of the experimental tensile test specimens. The procedure used is discussed in detail later in this paper.

6 ### 3. Experimental Procedure and Numerical Calculations

7   In this study, specimens were manufactured from DQA steel plate with a thickness of 14 mm as well
8 as from cold drawn bar (CDB) S355J2C+C with a diameter of 16 mm. The chemical compositions and mechanical
9 properties according to the material certificates for both steels are presented in Table 1 and
10   Table 2, respectively. The CEVs for DQA and CDB steels are 0.61 and 0.41, respectively. In
11   Table 2, $R_{p0.2}$ is the 0.2 % offset yield stress, f_u is ultimate tensile strength, A_t and A_5 are elongations at
12 fracture, Charpy-V -40 °C is the Charpy impact toughness value at -40 °C. Hardness values are measured by
13 manufacturer using Brinell hardness [HB].

14 Table 1. Chemical weight percent compositions according to the material certificates.

Steel	C [%]	Si [%]	Mn [%]	P [%]	S [%]	Al [%]	N [%]	Cu [%]	Cr [%]	Ni [%]	Mo [%]	Sn [%]	Fe
DQA	0.185	0.31	0.95	0.009	0.001	0.045	0.003	0.017	0.61	1.46	0.197	0.003	balance
CDB	0.15	0.22	1.29	0.012	0.022	0.022	-	0.25	0.09	0.09	0.03	-	balance

15
16 Table 2. Mechanical properties according to the material certificates.

| Steel	$R_{p0.2}$ [MPa]	f_u [MPa]	A_t [%]	A_5 [%]	Charpy-V -40 °C [J]	Hardness [HB]
DQA	1230	1497	9	-	71	462-472
CDB	650	695	-	12.8	-	209

17   Round notched tensile specimens and specimens with metallurgical constraints were used in this study.
18 The geometries of the notched specimens are presented in Figure 1. For specimens with geometry presented in
19 Figure 1 (a), UN is used as the abbreviation, and the notch radii presented in Figure 1 (b) and (c) are used hereafter
20 as the abbreviation for notched specimens.

21
22   (a)   (b)   (c)
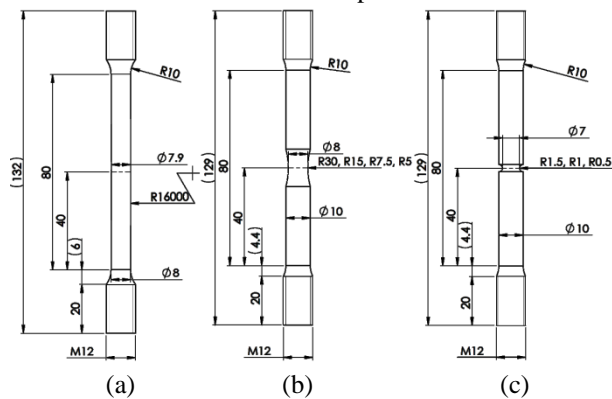
23 Figure 1. Geometries of the notched specimen. (a) geometry of specimens UN. In (b) geometry of specimens with
24 notch radiuses 30, 15, 7.5 and 5 mm and in (c) geometry of specimen with notch radiuses 1.5, 1 and 0.5 mm.

25   One specimen was manufactured from each material, respectively, for each notch radius except in the
26 case of DQA, from which two additional UN specimens were manufactured. In the case of DQA, square billets
27 with a length of 150 mm were saw-cut from a plasma-cut plate parallel to the rolling direction. The two additional
28 specimens, which are hereafter identified using the abbreviations UN45 and UN90, were manufactured with an
29 orientation of 45 and 90 degrees, respectively, to the rolling direction. A schematic representation of the billet
30 orientations is presented in Figure 2. Subsequently, the billets were turned to the given dimensions using a
31 numerically controlled (NC) lathe. The CDB specimens were saw-cut to a length of 150 mm and then turned using
32 an NC lathe. For both steels, specimens UN, R30, R7.5, R5, R1.5 and R0.5 were used to determine the Johnson-
33 Cook model material properties.

Use of the Quasi-Static Johnson-Cook Model in the Failure Assessment of Tensile Specimens With Metallurgical Constraints
Riku Neuvonen, Tuomas Skriko, Timo Björk

31.3.2020

1   Specimens R15 and R1 were not used in the material parameter identification process described later
2 and were instead used to verify the generated material model. Correspondingly, the DQA specimens UN45 and
3 UN90 were used to study the degree of anisotropy of the DQA plate.
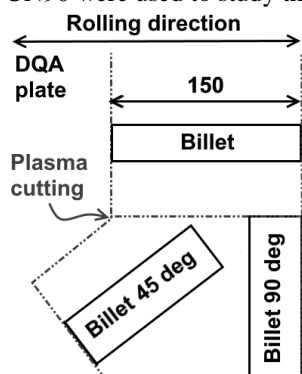
4
5 Figure 2. Schematic presentation of the DQA billet orientations.

6   Specimens with metallurgical constraints were manufactured by joining DQA billets and CDB billets
7 using rotational friction welding. The welding parameters and measured cooling time are presented in Table 3.
8 The parameters were chosen in order to minimize the heat input and thus minimize the metallurgical changes
9 occurring in the joint without compromising the strength of the weld interface. The DQA billets were kept
10 stationary during welding. A schematic representation of the manufacturing phases is presented in Figure 3,
11 whereby each number inside a square denotes a single phase. The abbreviation FWXX, whereby the XX is
12 replaced with the measured length between the weld interfaces, is used hereafter to identify the specimens.

13   First, a DQA billet was friction welded to CDB. After welding, the burr was removed by turning using
14 a manual lathe. After removal of the burr, the total length was measured to compensate for the changes generated
15 by the welding process. After the measurement, the specimen was saw-cut to the desired length in the second
16 phase of the manufacturing process. In the third phase, a second DQA billet was welded to the DQA-CDB billet.
17 A numerically controlled lathe was used in the fourth phase to turn the specimens to the final dimensions.
18 Specimen FW10.9 is presented in Figure 4.

19   Nine tensile specimens with different degrees of metallurgical constraint, achieved by varying the
20 length of the CDB zone, were manufactured for the study. After the fourth phase, the lengths between the weld
21 interfaces were measured from images acquired using a macroscope. A macroscopy image with the measurements
22 for FW9.1 is presented in Figure 5. The weld interfaces were easy to identify from the specimens due to the
23 different degrees of surface roughness, caused by the hardness change between the materials, after the turning.
24 The distance between the weld interfaces was determined based on the average of two length measurements.

25   In addition to the specimens described above, six specimens were manufactured to test the tensile
26 strength of the weld interface and to conduct the hardness measurements. In this study, the Vickers hardness
27 measurement method with 5 kg load (HV5) was used. Two of these specimens were manufactured by joining two
28 DQA billets, two specimens by joining two CDB billets, and two specimens by joining DQA and CDB billets
29 using the given friction welding parameters. These specimens are hereafter referenced using the abbreviations
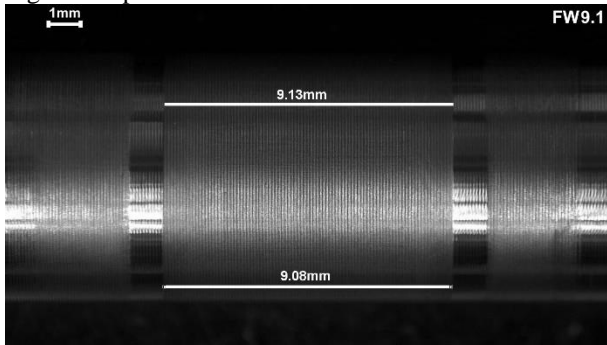30 DQA-DQA, CDB-CDB and CDB-DQA.

31 Table 3. Welding parameters.

Rotational speed [RPM]	Friction time [s]	Friction pressure [MPa]	Forging time [s]	Forging pressure [MPa]	Cooling time t_{8-5} [s]
1400	1.0	138	4	138	5
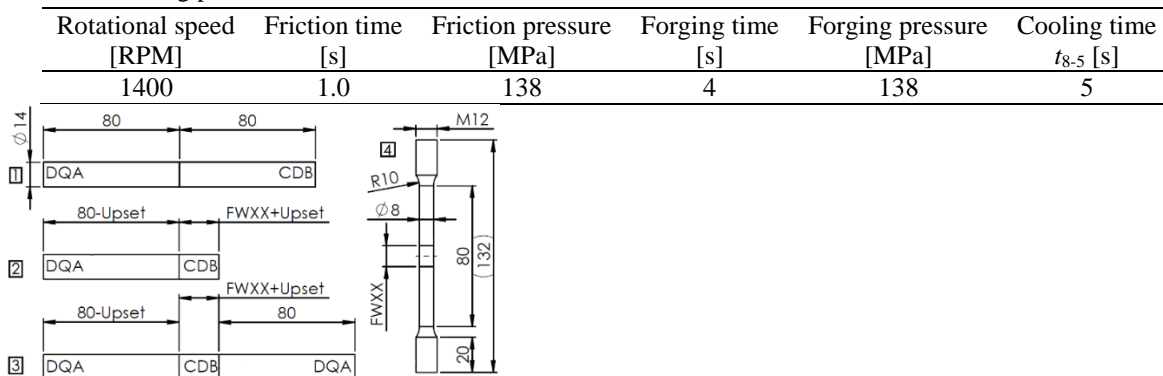
32
33 Figure 3. Schematic presentation of the manufacturing phases for specimens with metallurgical constraints.

Use of the Quasi-Static Johnson-Cook Model in the Failure
Assessment of Tensile Specimens With Metallurgical Constraints
Riku Neuvonen, Tuomas Skriko, Timo Björk

31.3.2020

1

2
3 Figure 4. Specimen FW10.9.

4
5 Figure 5. A macroscopy image of specimen FW9.1 with the measurement results.

6   Tensile tests were conducted for the specimens described above using a 150 kN servo-hydraulic test
7 rig with displacement control. The test setup is presented in Figure 6 (a). Cross head velocities used in the tensile
8 test and numerical calculations are presented in Table 4. In addition to a force sensor and a 50 mm strain
9 extensimeter, digital image correlation (DIC) 3D strain measurement equipment, known as ARAMIS, was used
10 to record the displacement data during the experiment. Prior to testing, the ARAMIS equipment was calibrated
11 using the procedure recommended by the manufacturer. The procedure involves a use of calibration panel. The
12 calibration was done for 75 mm lens with measuring volume of 105/80/60 mm. Single snap mode was utilized
13 with ellipse quality of 0.4. Calibration deviation was 0.03 pixels and the limit value according to the manufacturer
14 is 0.05 pixels. The scale deviation limit is 0.008 and the calibration result was 0.000 mm. During the measurement,
15 subsets or edge tracing was not used. A speckle pattern was applied to the surface of each specimen. Firstly
16 specimen was spray painted using a white color after that a black spray paint was used in order to generate the
17 pattern. An example of the used pattern in presented in Figure 6 (d). Due to the round geometry the light provided
18 by the measurement system creates a shadow to the edges, as can been seen from Figure 6 (d). Thus the pattern is
19 not as recognizable at the edges, thus creating problems and possible some noise to deformation data at the edges.

20   GOM Correlate software was used in order acquire the data from the experiments. A data point of DQA
21 UN specimen and a data point of FW4.9 is presented in Figure 6 (b) and (c), respectively. Firstly, a coordinate
22 system was aligned to the images captured from experiments. The Y-axis was designed to represent the axial
23 dimension of the specimen. In the case of notched tensile specimens, a fitting circle was added by selecting the
24 elements in the center line of the notch. A Gaussian best-fit method was applied and the normal of the generated
25 circle was forced to align with the Y-axis of the coordinate system. This circle, named minCC_YMP 1 in the
26 Figure 6 (b), was used to measure the minimum cross-section of the specimen. Five additional fitting circles,
27 1mm_YMP 1, 2mm_YMP 1, 3mm_YMP 1, 10mm_YMP 1 and 15mm_YMP 1, were also generated. The location
28 of these circles were measured from the minCC_YMP 1 in the undeformed state. As the specimen deformed, the
29 length between five additional circles and minCC_YMP 1 circle increased. The applied force was inputted to the
30 software as a voltage signal from the force sensor. The deformation data and force data was used in order to
31 generate force-displacement plots for the specimens.

32   After the alignment of the coordinate system, the next step in the post processing of the ARAMIS data
33 of the friction welded specimens was to determine the center line of the soft zone. This was done by analyzing the
34 Y-strain data. Symmetric deformation was assumed and thus, by knowing the length between the weld interfaces,
35 the center could be determined. A Gaussian best-fit circle, named WM_center_YMP 1 in Figure 6 (c), was
36 generated to that location. In addition, 15mm_YMP 1 was generated and the length between these circles and the
37 voltage data from the force sensor was used to generate the force-displacement data.

38   The numerical calculations were conducted using the FE software LS-Dyna. The axisymmetric model
39 of specimen UN is presented in Figure 7 (a). An examples of the models of the notched specimen and friction
40 welded specimen are presented in Figure 7 (b) and (c), respectively. All models were generated using nominal

1   diameters and notch radii. The lengths for the FWXX/2 of CDB in the models were adjusted according to the
2   measurements conducted for the specimens. In the FWXX models, the material parameters obtained using the
3   optimization routine described below were used. According to the metallographic examinations (for more details,
4   see the Results section), a straight weld interface was modeled. The HAZs of both materials were neglected in the
5   analysis models based on the hardness measurements and tensile tests conducted for the DQA-DQA, CDB-CDB
6   and CDB-DQA specimens; for more details, see the Results section.

7
8   (a)

9
10   (b)   (c)   (d)
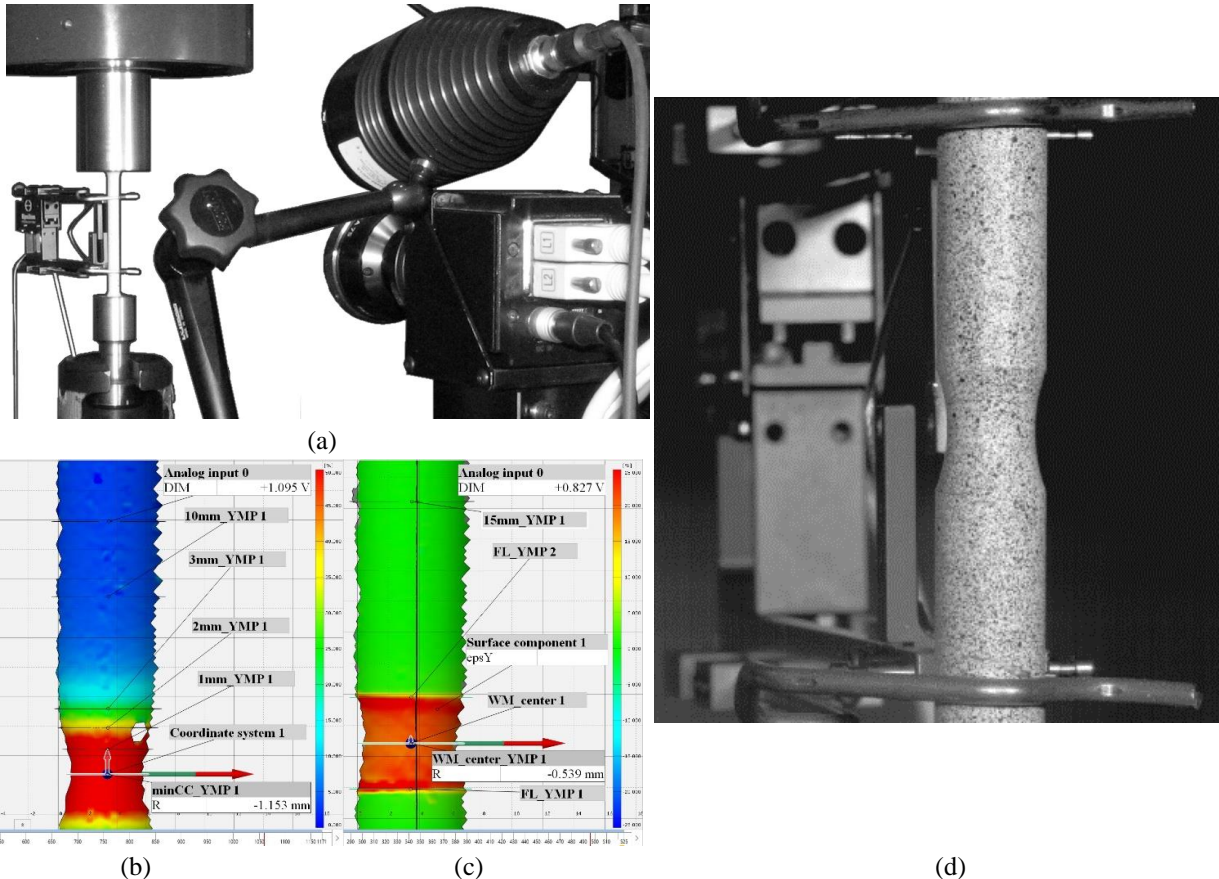
11   Figure 6. (a) Tensile test setup. Examples of data acquisitions from (b) a notched tensile specimens and from (c)
12   specimens with metallurgical constraint by utilizing GOM Correlate software. Example of the speckle pattern
13   applied to the surface of specimens for DIC. Color contours in (b) and (c) represent the axial strains of the
14   specimens.

15   Symmetrical constraints were used in the symmetry planes, represented by the dotted lines in Figure 7.
16   Displacement as a function of time, represented by the arrows in Figure 7, was added to simulate the movement
17   generated by the tensile test machine. The mesh was generated using fully integrated (four integration points
18   through thickness) volume weighted axisymmetric solid elements (ELFORM 15 in LS-Dyna) with LS-Dyna
19   default viscous hourglass control.

20   The size of the fine mesh at the axial symmetry end of the models was 0.1*0.1 mm. It is clear that the
21   mesh size and the shape of the elements had an effect on the results, especially beyond uniform elongation. When
22   necking begins, strain localizes to a certain region. Since the strain values after localization are dependent on the
23   gauge length, the values differ depending on the mesh size. The authors acknowledge this fact, but since the
24   dependency of the mesh size is not the focus of this paper, only the stated mesh size was used in the calculations.

25   An explicit solver was used to solve the models. The displacement speed used in the models was equal
26   to the crosshead speed of the tensile test for the given specimen. Mass scaling (in LS-Dyna setup, DT2MS value
27   was set to 5) was used to increase the stable time step of the explicit formulation in order to reduce the
28   computational time without compromising the results. The energy balance of each simulation was analyzed to
29   ensure that the amount of kinetic or hourglass energy was negligible.

Use of the Quasi-Static Johnson-Cook Model in the Failure
Assessment of Tensile Specimens With Metallurgical Constraints
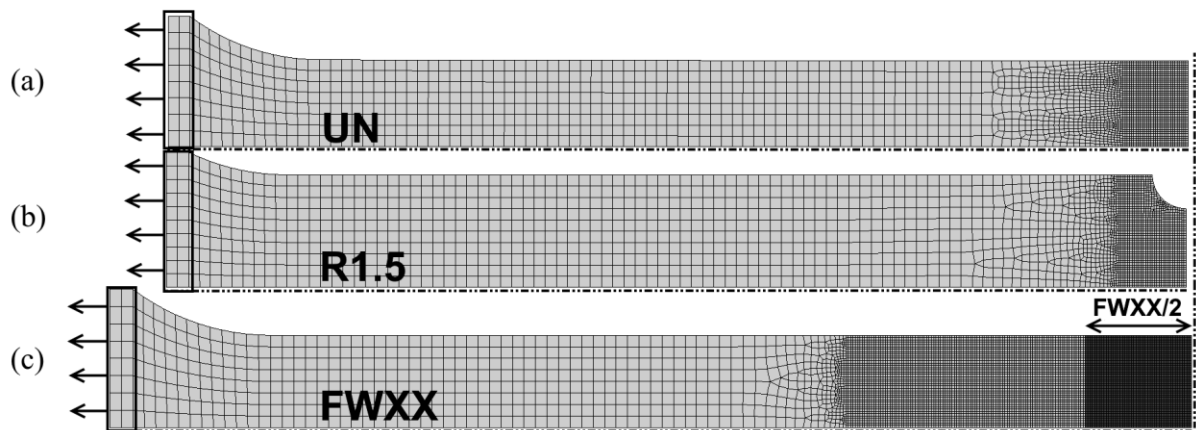Riku Neuvonen, Tuomas Skriko, Timo Björk

31.3.2020

Figure 7. (a) FE model used for UN specimens. (b) Example of the FE model for notched specimens and (c) example of FE model for friction welded specimens.

Table 4. Cross head velocities used in the experiments and in FE calculations.

Specimen	Cross head velocity [mm/s]	Specimen	Cross head velocity [mm/s]	Specimen	Cross head velocity [mm/s]
DQA UN	0.006	CDB UN	0.01	FW19.1	0.005
DQAUN45	0.006	CDB R30	0.008	FW14.6	0.005
DQA UN90	0.006	CDB R15	0.006	FW10.9	0.005
DQA R30	0.004	CDB R7.5	0.004	FW9.1	0.004
DQA R15	0.0035	CDB R5	0.004	FW6.8	0.004
DQA R7.5	0.003	CDB R1.5	0.003	FW4.9	0.004
DQA R5	0.003	CDB R1	0.003	FW4.0	0.003
DQA R1.5	0.003	CDB R0.5	0.003	FW2.8	0.0025
DQA R1	0.003			FW2.2	0.0025
DQA R0.5	0.0025				

The material parameters for both steels used in this study were obtained using an optimization routine generated for the optimization software LS-Opt. In this study, metamodel-based optimization using a sequential optimization strategy with domain reduction was used. The routine determines the values for the chosen continuous variables used in the FE models and compares the numerical results to the imported experimental results. The routine is iterative and after each iteration loop, the values used for the variables are adjusted according to the previous results until the converged solution fulfils the inputted termination criteria. For the first iteration round, the user must input the initial values for the variables in addition to the limiting values. Material model parameters to be determined were inputted into the optimization routine as continuous variables.

The parameter identification was done for both applied materials in two phases using the tensile test results and FE models of specimens UN, R30, R7.5, R5, R1.5 and R0.5. In the first phase, the parameters A, B and n were determined. In this phase LS-Dyna material model MAT_098 was used. The experimental force-displacement curves obtained from the DIC measurements were used as input data for the optimization. An example of the input data obtained from the tensile test of the specimen CDB UN used in optimization of parameters A, B and n is presented in Figure 8 (a). The curves represent the different gauge lengths. The numerical values of force and displacement were adjusted for the axisymmetric condition of the FE models.

The parameters D_1, D_2 and D_3 were determined in the second optimization phase. Since in LS-Dyna MAT_098 ignores failure the material model was changed to MAT_015 in LS-Dyna. MAT_015 was used in analysis where parameters D_1, D_2 and D_3 was utilized. In these calculations, the constitutive parameters determined in the first optimization phase were used as material constants. In order to identify the fracture parameters, the optimization routine requires input data regarding the fracture. In this study, the instantaneous radius of the minimum cross-section displacement curves presented in Figure 8 (b) was used as the input data for the optimization. The curves were constructed by combining the FE results using the optimized constitutive model parameters with the measured fracture radii of the tensile specimens. The diameter was constant after the fracture; thus, after the ultimate displacement, the diameter was set to the measured value. This procedure was chosen

Use of the Quasi-Static Johnson-Cook Model in the Failure
Assessment of Tensile Specimens With Metallurgical Constraints
Riku Neuvonen, Tuomas Skriko, Timo Björk

31.3.2020

1 because the exact point of fracture initiation could not be determined from the tensile tests and because the FE
2 results were in good agreement with the experimental data; for more details, see the Results section.
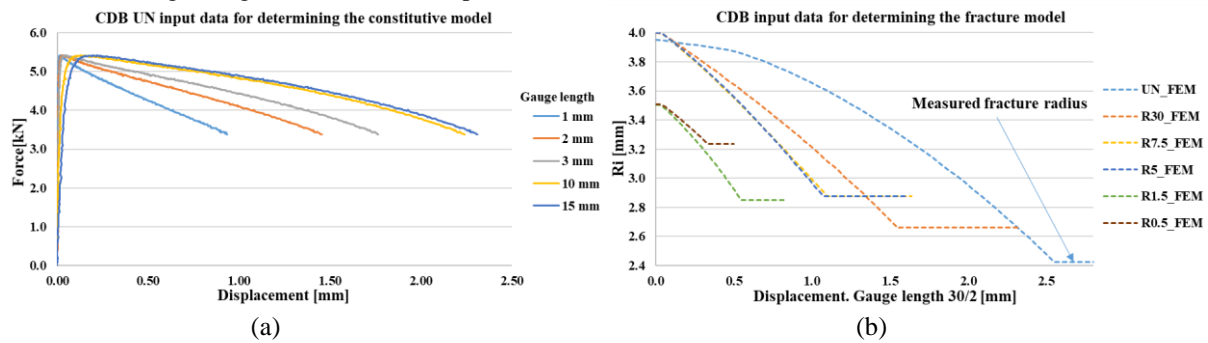
3
4   (a)   (b)
5 Figure 8. Example of the input data for the optimization of the material parameters. Experimentally determined
6 values have been adjusted for the axisymmetric condition.

7 ### 4. Results

8   The hardness measurements conducted for near-surface and middle of the specimen CDB-DQA are
9 presented in Figure 9 (a) and (b), respectively. According to the measurements, the HAZ in DQA has a distinct
10 softened zone, which is typical for DQ steels. The lowest hardness is approximately 300 HV5, which is in the
11 order of 75 % of the pure/unaffected base material hardness. The measured hardness values of the CDB bar in
12 welded condition varied by approximately ±10 % compared to the hardness value given in the material certificate.
13 Since hardness was nearly constant in the CDB, it was assumed that the CDB part of the specimen with
14 metallurgical constraints could be modelled using the material properties obtained from the notched CDB
15 specimens.

16   The tensile test results for the DQA-DQA, CDB-CDB, and CDB-DQA specimens are presented in
17 Figure 10. In the DQA-DQA specimens, the fracture occurred in the softened HAZ. Both the CDB-CDB and
18 CDB-DQA specimens fractured at the base material outside the gauge length. Thus, the fracture occurred more
19 than 25 mm from the weld interface, clearly outside the HAZ, which indicates that the HAZ has a strength that is
20 at least equal to that of the base material. Due to the higher hardness and tensile strength of the DQA HAZ
21 compared to the CDB, the softened HAZ was also modelled using DQA material properties obtained from the
22 optimization.

23   The weld interface was examined in detail using scanning electron microscopy (SEM) and energy-
24 dispersive X-ray spectroscopy (EDS) analyses. The CDB and DQA can be distinguished from each other by the
25 percentage of elements Cr and Ni. Figure 11 presents the EDS analysis of these elements at the weld interface. A
26 distinct weld interface and a clear difference in the amounts of these elements can be observed in Figure 11. The
27 width of each contour map is approximately 60 µm. The FE model was generated with a 100 µm mesh size. Thus,
28 the existence of a clear and sharp interface between the materials in the FE model was assumed.
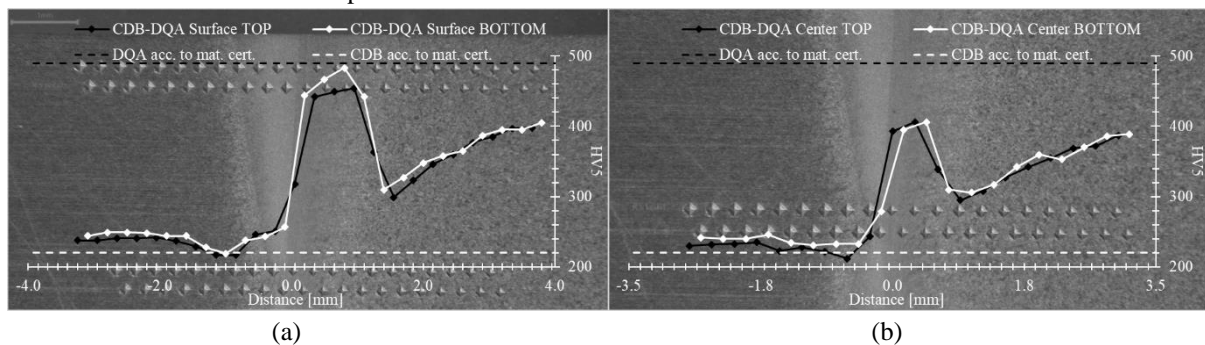
29
30   (a)   (b)
31 Figure 9. Hardness distributions from (a) near-surface and (b) middle of the CDB-DQA friction welded joint.

**Use of the Quasi-Static Johnson-Cook Model in the Failure
Assessment of Tensile Specimens With Metallurgical Constraints**
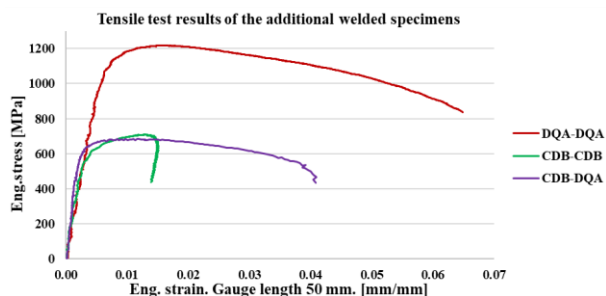Riku Neuvonen, Tuomas Skriko, Timo Björk

31.3.2020

1

2 Figure 10. Tensile test results of the additional specimens.
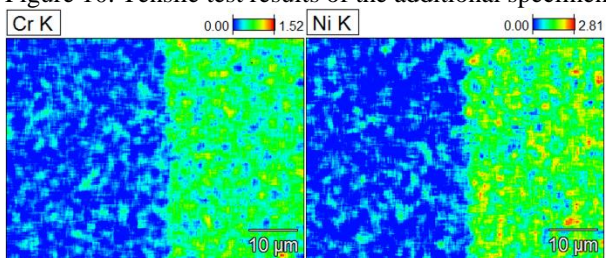
3

4 Figure 11. EDS contour map of the Cr and Ni contents at the weld interface of the CDB-DQA friction welded
5 joint.

6   The tensile test results of the DQA UN specimens with different orientations are presented in Figure
7 12. The ultimate strength of the three specimens varied by 3.2 % and the difference in the minimum diameter after
8 fracture was 10.7 %. The difference in the tensile behavior was small. According to these results, the DQA
9 material might be slightly anisotropic. The specimens with metallurgical constraints were manufactured from
10 billets cut parallel to the rolling direction, and the material parameters for DQA were defined using specimens
11 with the same orientation. In addition, the results from the FE calculations were in good agreement with the test
12 results without applying the anisotropic material model. Thus, anisotropy was neglected in this study. The same
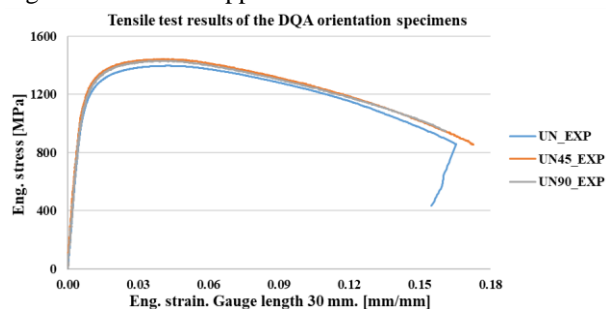13 argumentation was applied for the CDB material.

14

15 Figure 12. Experimental tensile test results of the DQA UN specimens with different orientation.

16   4.1. Notched tensile specimens

17   The fracture surfaces of all notched specimens are presented in Figure 13. Ductile fractures can be
18 observed in all specimens. The material parameters obtained from the optimization routine are presented in Table
19 5. Strain rate and temperature effects were suppressed in the material model by using suitable predetermined
20 parameters presented in Table 5. Graphical presentation of constitutive and fracture models for the used steels are
21 presented in Figure 14 (a) and (b), respectively. In Figure 15 (a) and (b), a comparison between the diameter
22 reduction in CDB and DQA specimens and the FE models is presented, respectively. The FE results are in good
23 agreement with the experimental data. As the fracture model parameters do not influence the diameter reduction
24 prior to element erosion, the calculated results combined with the experimentally determined fracture radii can be
25 used in the identification of the damage parameters.

26   The stress-strain results of CDB specimens used in the optimization and the corresponding numerical
27 results are presented in Figure 16 (a). In Figure 16 (b), the stress-strain results of CDB specimens not used in
28 optimization and the corresponding numerical results are presented. The stress-strain results obtained from tests
29 with DQA specimens and the corresponding FE results used in optimization are presented in Figure 16 (c) and
30 the stress-strain results of DQA specimens not used in optimization and the corresponding FE results are presented

Use of the Quasi-Static Johnson-Cook Model in the Failure
Assessment of Tensile Specimens With Metallurgical Constraints
Riku Neuvonen, Tuomas Skriko, Timo Björk

31.3.2020

1   in Figure 16 (d). A detailed comparison of the percentage difference in the ultimate tensile strength and diameter
2   after fracture is presented in Table 6. In the table, the dashed lines separate the specimens not used in the
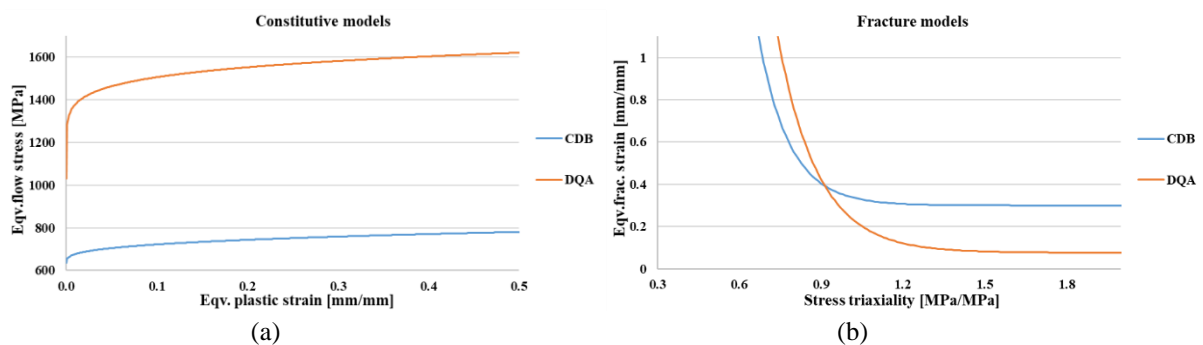3   optimization. The FE modelling results are in good agreement with the experimental data.
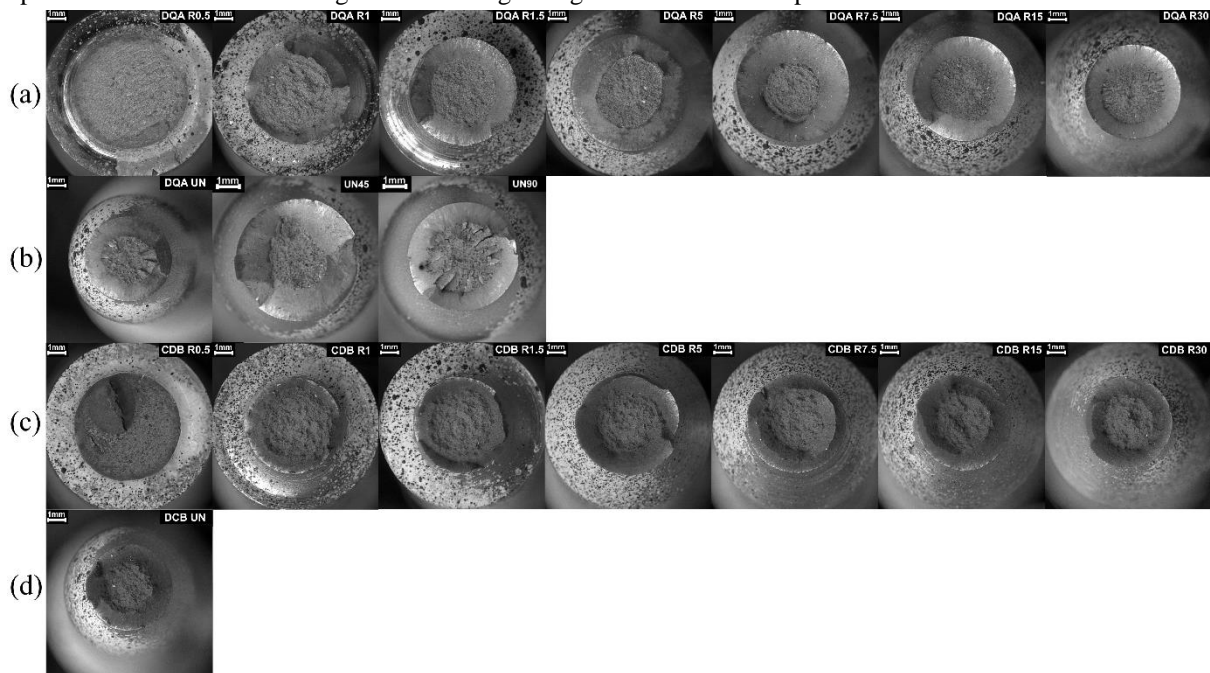
4
5   Figure 13. Fracture surfaces of notched specimens. Row (a): DQA specimens in ascending order from R0.5 to
6   R30. Row (b): DQA UN, UN45 and UN90. Row (c): CDB specimens in descending order from R0.5 to R30. Row
7   (d): CDB UN.

8   Table 5. Predetermined material parameters and parameters obtained from the optimization.

Steel	A [MPa]	B [MPA]	n	D_1	D_2	D_3
CDB	636.679	180.122	0.325815	0.299891	305.29	-8.85566
DQA	1030.61	648.548	0.13464	0.075977	156.687	-6.78667
Predetermined material parameters	C=0	m=1	D_4=0	D_5=0	T_{ref}=200 K	T_{melt}=1*10^{20} K

9

10   (a)   (b)
11
12   Figure 14. (a) Constitutive and (b) fracture models for the used steels.

Use of the Quasi-Static Johnson-Cook Model in the Failure
Assessment of Tensile Specimens With Metallurgical Constraints
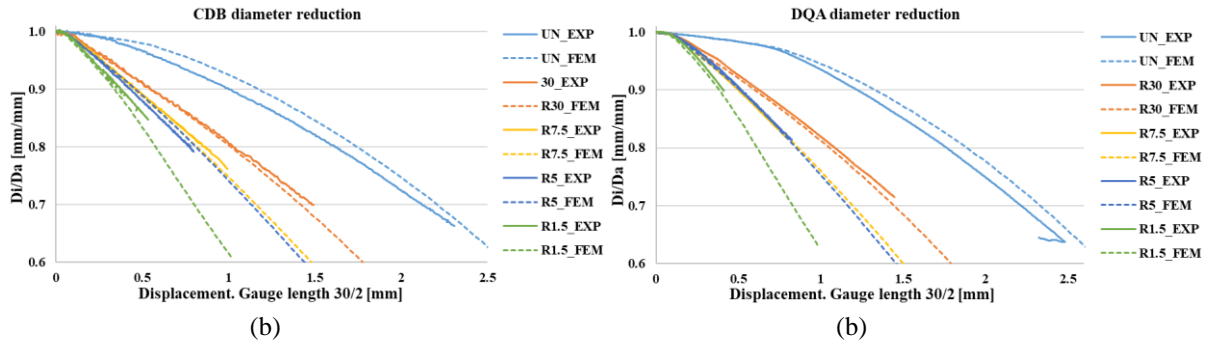Riku Neuvonen, Tuomas Skriko, Timo Björk

31.3.2020

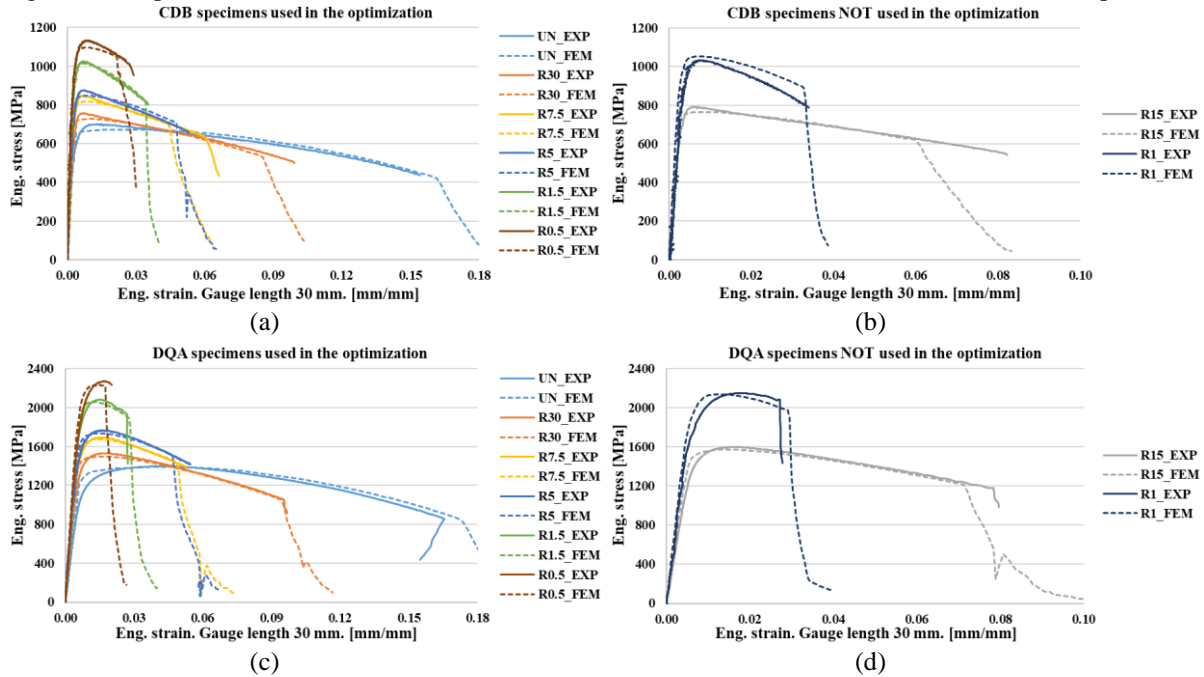Figure 15. Experimental (EXP) and FE results of the diameter reduction in (a) CDB and (b) DQA specimens.

Figure 16. Comparison of the stress-strain curves from the experimental tests and FE modellings.
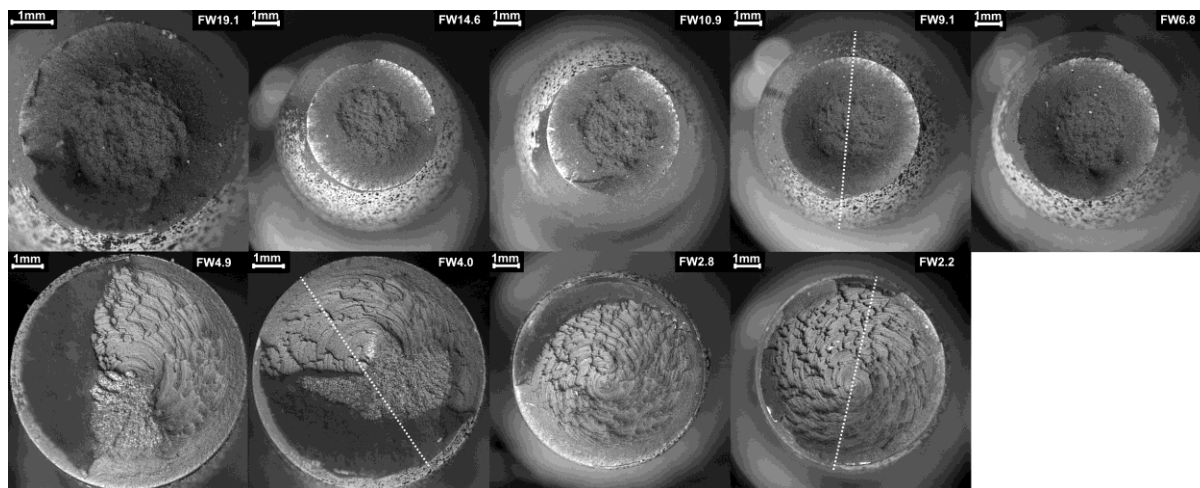
Table 6. Percentage difference between the experimental values and FE results.

| Specimen	Tensile strength		Diameter after fracture	
	CDB [%]	DQA [%]	CDB [%]	DQA [%]
UN	-4.3	-0.5	-5.6	-3.8
R30	-4.2	-2.0	-0.7	-6.8
R15	-3.4	-1.6	5.7	-16.2
R7.5	-3.8	-1.1	5.8	-5.2
R5	-3.3	-1.7	6.1	-4.0
R1.5	-1.0	-0.8	-1.0	0.2
R1	2.0	-0.2	9.1	-3.1
R0.5	-2.7	-1.2	-1.7	1.6

4.2. Specimens with metallurgical constraints

The fracture surfaces of specimens with metallurgical constraints are presented in Figure 17. A cup and cone fracture mechanism at the center of the CDB region was observed in specimens FW19.1, FW14.6, FW10.9, FW9.1 and FW6.8. Specimens FW4.9, FW4.0, FW2.8 and FW2.2 fractured near the weld interface. In Figure 18, the cross-sections of the fractured specimens FW9.1, FW4.0 and FW2.2 are presented. The orientations of the cross-section images are represented by dashed lines in Figure 17.

Use of the Quasi-Static Johnson-Cook Model in the Failure
Assessment of Tensile Specimens With Metallurgical Constraints
Riku Neuvonen, Tuomas Skriko, Timo Björk

31.3.2020

1   The experimentally and numerically obtained stress-strain curves of specimens fractured via cup and
2   cone mechanism are presented in Figure 19 (a) and (b). In Figure 19 (c) and (d), the corresponding results from
3   specimens fractured near weld interface are presented. According to the figure, the tensile strength of the specimen
4   increases as the width of the CDB zone decreases. The nominal mismatch of the friction welded joint is
5    $M_n = f_{u.CDB}/f_{u.DQA} = 0.46$. According to the tensile test results of the UN specimens, the mismatch is $M_e = f_{u.CDB}$
6    $_{UN}/f_{u.DQA\ UN} = 0.50$. The mismatch for each specimen can be defined as $M_{FWXX} = f_{u.FWXX}/f_{u.DQA\ UN}$. Figure 20 presents
7   the values of M_{FWXX} versus the length between the weld interfaces (L_{FL}) divided by the original diameter (D_a) of
8   the specimen. The increase in the tensile strength is due to the increase in the metallurgical constraints as the $L_{FL}/$
9   D_a value decreases.

10

11

12   Figure 17. Fracture surfaces of the specimens with metallurgical constraints.
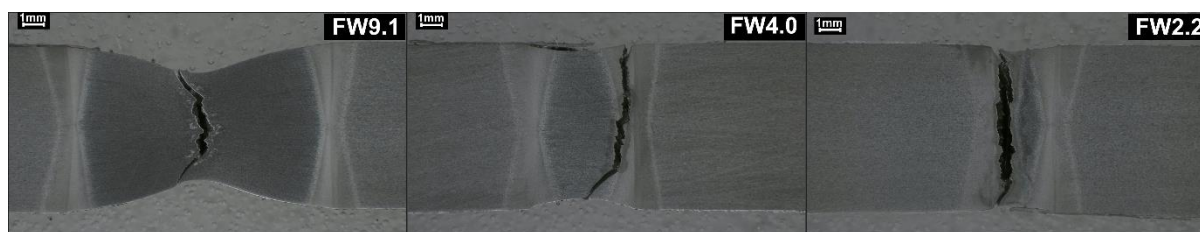
13

14   Figure 18. Cross-sections of the fractured specimens FW9.1, FW4.0 and FW2.2.

15   The percentage difference between the experimental results and the FE modellings for tensile strength
16   and displacement at fracture measured by 30 mm gauge length are presented in Table 7. In the tests, the actual
17   fracture initiation points could not be determined. Thus, the last recorded displacement value was used to represent
18   the values. In the FE results, the fracture point was determined when the value of D in the first element was equal
19   to 1. The FE model contours of parameter D at the instance of the erosion of the first elements are presented in
20   Figure 21. The red dashed lines represent the weld interfaces and the white arrows point to the location of fracture
21   initiation. The fracture initiated at the center of the axial symmetry plane (center of the CDB region) in models
22   FW19.1, FW14.6, FW10.9, FW9.1 and FW6.8. The fracture initiated at the weld interface at the surface in models
23   FW4.9, FW4.0, FW2.8 and FW2.2. Thus, the experimental results of the two distinct fracture locations were
24   matched by the FE models. The numerically obtained results are in good agreement with the experimental results
25   for the specimens fractured by the cup and cone mechanism.
26   In Figure 22 (a) and (b), the effective plastic strain contours of FE models are presented for cup and
27   cone fracture and fracture near the weld interface, respectively. In the case of cup and cone fracture, the effective
28   plastic strain has the highest value at the center of the model. As L_{FL}/D_a ratio decreases, the effective plastic strain
29   starts to accumulate to CDB side of weld interface at the surface of the specimen.
30   Figure 23 (a) and (b) present the contours of stress triaxiality of FE models. In addition to the increased
31   stress triaxiality at the center of the notch, a concentration of stress triaxiality can be observed at the weld interface

Use of the Quasi-Static Johnson-Cook Model in the Failure
Assessment of Tensile Specimens With Metallurgical Constraints
Riku Neuvonen, Tuomas Skriko, Timo Björk

31.3.2020

1   in the surface of the soft zone. The location of increased stress triaxiality occurs in the same location as maximum
2   effective plastic strain in specimens fractured near weld interface, see Figure 22 (b).
3   The Lode parameter contours of FE models fractured via cup and cone mechanism are presented in
4   Figure 24 (a). In the Figure 24 (a), the Lode parameter contour indicates that stress state in the center of specimens
5   correspond to axisymmetric uniaxial tension. At the surface, the L value is slightly lower than 1. In the surface of
6   the soft zone at the weld interface, there is a region of plane strain, i.e. $L=0$. Plane strain stress state can be observed
7   also in the FE models fractured near the weld interface, see Figure 24 (b). In the center of the notch, the area under
8   axisymmetric tension seems to be reduced as the ratio L_{FL}/D_a decreases and the stress state at surface is shifted
9   towards the plane strain condition.

10
11   (a)   (b)
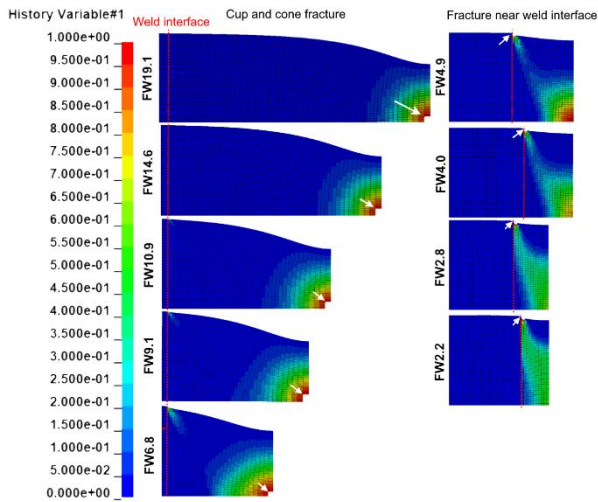
12
13   (c)   (d)
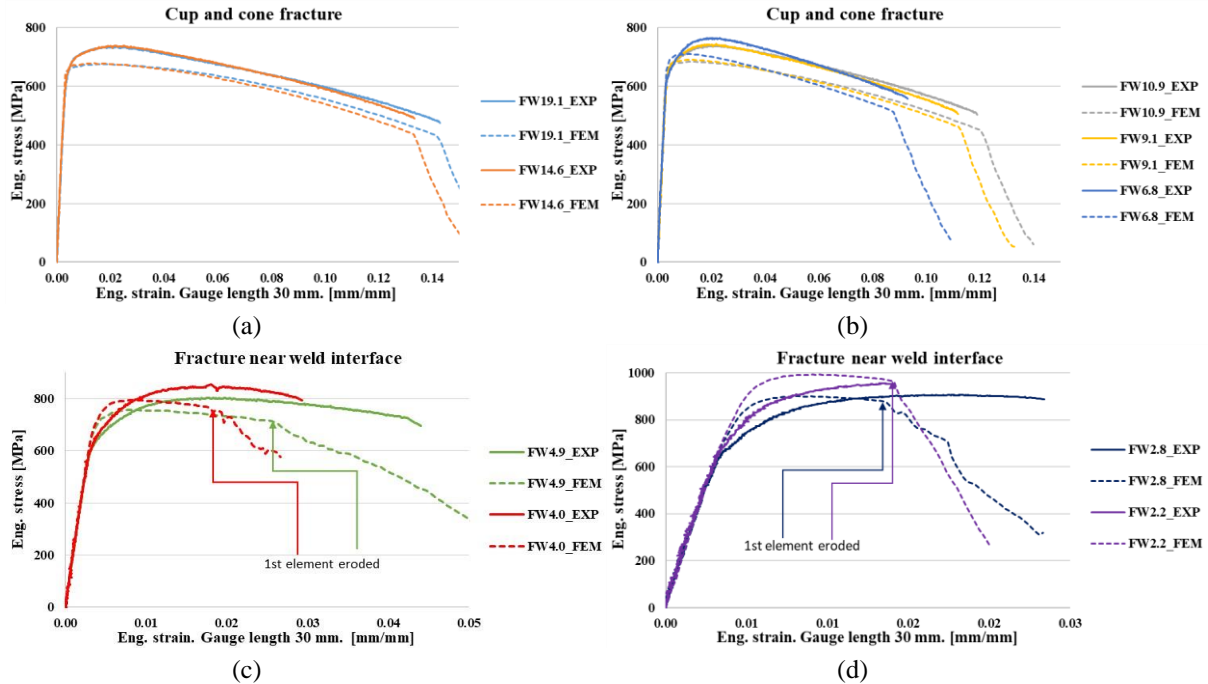
14 Figure 19. Comparison between the stress-strain curves from the experimental tests and the FE modellings of the
15 specimens with metallurgical constraints.

16
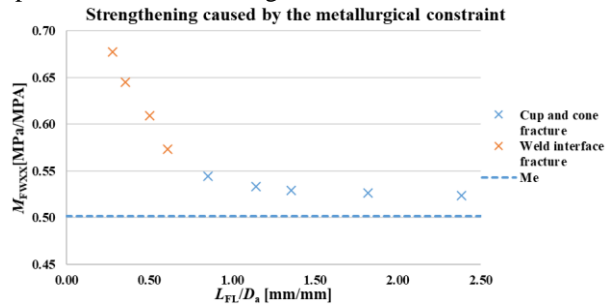
17 Figure 20. Tensile strength mismatch of each specimen versus L_{FL}/D_a.

18 Table 7. Percentage difference between the experimental values and FE results of the specimens with metallurgical
19 constraints.

	Cup and cone fracture					Fracture near weld interface			
	FW19.1	FW14.6	FW10.9	FW9.1	FW6.8	FW4.9	FW4.0	FW2.8	FW2.2
Diff. f_u [%]	-8.4	-8.5	-7.9	-7.9	-7.2	-5.7	-7.0	-0.2	4.6
Diff. δ_{30} [%]	-0.6	0.0	1.3	0.7	-6.6	-71.2	-61.8	-68.1	-0.3

Use of the Quasi-Static Johnson-Cook Model in the Failure
Assessment of Tensile Specimens With Metallurgical Constraints
Riku Neuvonen, Tuomas Skriko, Timo Björk

31.3.2020

Figure 21. Damage contours of the FE models of the specimens with metallurgical constraints. Images are taken after the first elements have been eroded.

(a)   (b)
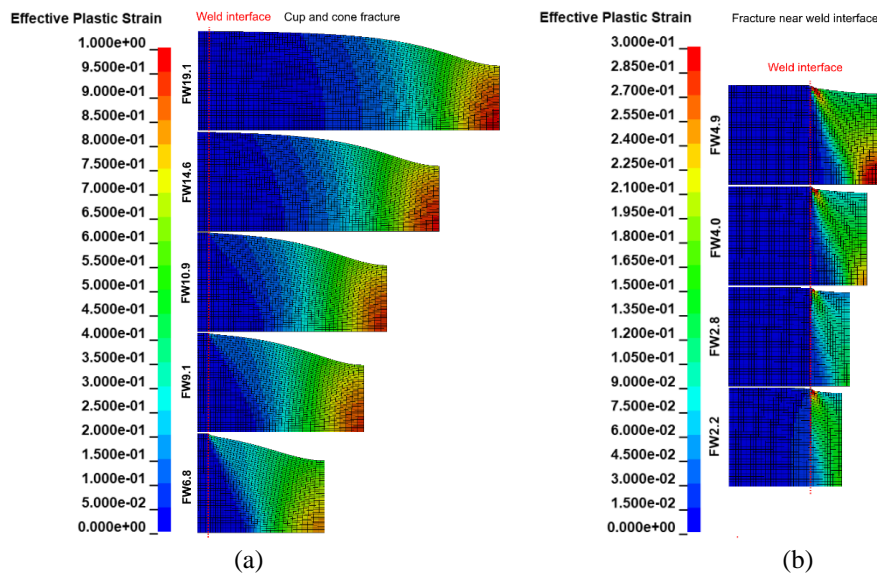
Figure 22. Effective plastic strain contours of FE models with (a) cup and cone fracture and (b) fracture near weld interface. Images are taken a single time step prior the first elements have been eroded.

(a)   (b)
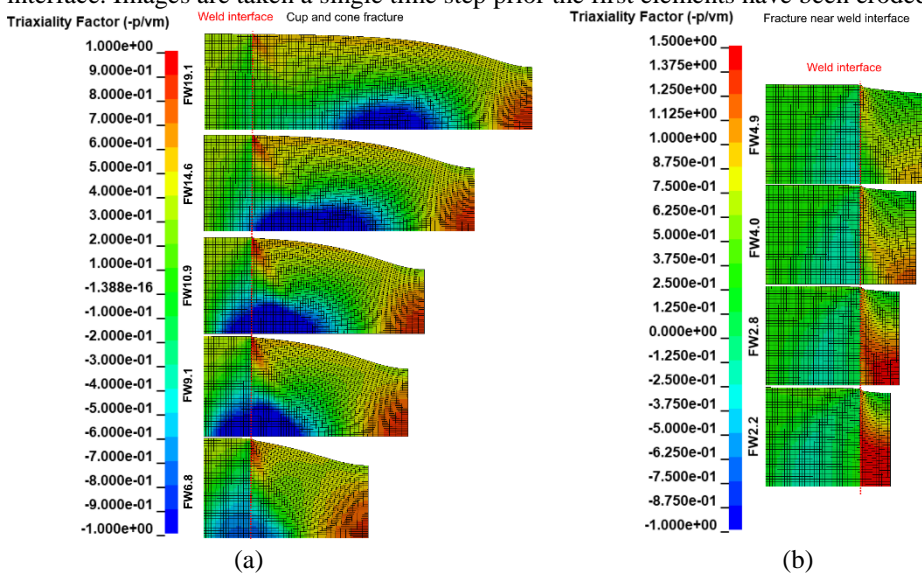
Figure 23. Stress triaxiality contours of FE models with (a) cup and cone fracture and (b) fracture near weld interface. Images are taken a single time step prior the first elements have been eroded.

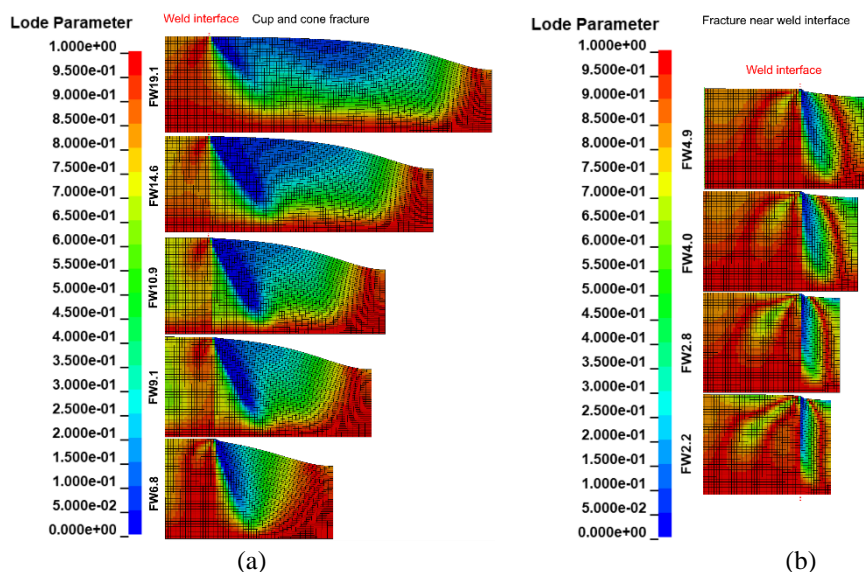(a)   (b)

Figure 24. Lode parameter contours of FE models with (a) cup and cone fracture and (b) fracture near weld
interface. Images are taken a single time step prior the first elements have been eroded.

5. Discussion

A good agreement between the experimental tensile test results and FE calculations was achieved using
the Johnson-Cook model with material parameters obtained using the optimization routine. Thus, the model can
estimate the behavior of DQA and CDB steels in the quasi-static region for round specimens. In the introduction
section, the issues concerning the soft zone in weldments of DQ steels were discussed. The material models were
calibrated to study the possibility of using the Johnson-Cook material model to assess the effects of a softened
zone on the load-carrying and deformation capacity under the given circumstances. Because metallurgically
induced changes in the mechanical properties of the HAZ in DQ welds can be very complex, simplified specimens
were manufactured using friction welding. A distinct weld interface was observed between the materials. The
hardness values of the CDB only changed by ±10 % and thus, it was assumed that the CDB region can be modelled
using the identified parameters.

According to Porter [6], DQ steels are prone to softening in the HAZ. This behavior was also observed
in this study. Experimental tensile tests conducted for the CDB-CDB, CDB-DQA and DQA-DQA specimens
showed that the tensile strength of the DQA-DQA specimens is approximately 500 MPa greater than the tensile
strength of CDB. Thus, the softened zone of the DQA in the FE models generated for the specimens was neglected
and the model was generated using the obtained parameters.

Sun et al. [9] used analytical and FE calculations based on experiments conducted by Ran et al. [8] to
predict the strength increase caused by the metallurgical constraints in the axisymmetric condition. In this study,
the strengthening phenomenon was observed directly from the tensile experiments; see Figure 20. However, the
results obtained by Sun et al. [9] and achieved in this study are not directly comparable because of the difference
in the strength values of the used materials. Both studies indicate that if the numerical value of the width of the
soft zone divided by the diameter is less than 1.0, the effect of the metallurgical constraints starts to increase, and
when the value is in the order of 0.5, the effect intensifies.

Ran et al. [8] reported that mechanical properties and the width of the soft zone govern the overall
behavior of the joint. They noticed that as the width of the soft zone decreases, the strength increases. In the
current study, the tensile strength of the specimens with metallurgical constraints increased and the ductility
decreased as the length of the soft region decreased.

In this study, two different fracture behaviors were observed. The specimens with an L_{FL}/D_A ratio
greater than 0.8 fractured from the center of the CDB zone by the cup and cone mechanism. The specimens with
an L_{FL}/D_A ratio smaller than 0.6 fractured near the weld interface. Fusion line fracture of ultra-high strength steel
weldments has previously been reported by Björk et al. [11] in fillet welded joints. As the L_{FL}/D_A ratio decreased
from 0.85 to 0.61 mm, the fracture location shifted from the center of the softened region to the weld interface,
the ultimate strength of the specimens increased by 5 %, and the elongation at fracture decreased by 54 %.

Use of the Quasi-Static Johnson-Cook Model in the Failure
Assessment of Tensile Specimens With Metallurgical Constraints
Riku Neuvonen, Tuomas Skriko, Timo Björk

31.3.2020

1   In order to design and manufacture safe steel structures, the ductility and strength of welds must be at
2   a sufficient level. Skriko [12] noted that on the basis of proper manufacturing parameters, e.g. heat input and
3   groove preparation, joints with suitable performance quality can be fabricated from S960 DQ steel. The results of
4   this study indicate that, at least under the given conditions, there is a certain cut-off value where the ductility of
5   the joint decreases suddenly while the strength increases only slightly. Despite the limited amount of specimens
6   and stress states covered in this study, it seems that the softening phenomenon must be considered in order to
7   manufacture joints with suitable strength and ductility from DQA steels. Further studies must be conducted to
8   gain more information on this phenomenon before any firm conclusions can be drawn.
9   Both Rodriques et al. [10] and Sun et al. [9] concluded that the width of the softened zone, the mismatch
10   ratio, and the hardening parameters of the adjacent materials affect the metallurgical constraints and the tensile
11   properties of the joint. According to Figure 16 and Table 6, the use of the optimization routine generated reliable
12   hardening parameters for the materials used in the specimens with metallurgical constraints. Also, both the width
13   and the geometry of the softened zone and the mismatch ratio were clearly defined in this study. This seems to
14   indicate that these parameters govern the mechanical behavior of specimens with metallurgical constraints.
15   The FE calculations of specimens with metallurgical constraints were in good agreement with the
16   experimental results for the specimens with a cup and cone fracture, but they underestimated the fracture
17   displacement when the fracture occurred near the weld interface. The difference between the predicted and tested
18   tensile strengths shows a clear trend, namely it increased as the length of the soft region decreased. A reason for
19   this could be that the models overestimated the metallurgical constraints because the softened HAZ of the DQA
20   was neglected. The decision to omit the soft HAZ was made based on the hardness and tensile test results for the
21   DQA-DQA, CDB-CDB and DQA-CDB specimens. However, in the DQA-DQA specimens, there is also the
22   possibility that the metallurgical constraints strengthened the soft zone and thus, affected the results by increasing
23   the tensile strength.
24   Since the DQA HAZ was not studied in detail, no information about the constitutive behavior of HAZ
25   is currently available. The hardness distribution in HAZ is not constant; thus, the discretization of the mechanical
26   properties for the whole zone is not a trivial task. In addition, as has been discussed, reliable material parameters
27   need to be used when studying the metallurgical constraint effect. In order to improve the results, the different
28   regions of HAZ must be included in the models, and consequently, further research in terms of this topic is needed.
29   As mentioned before, the fracture model used in this study does not include the influence of the Lode
30   parameter. According to Figure 24 (b) there is a local plain strain condition in the location of fracture initiation in
31   addition to an elevated stress triaxiality value. According to literature [27, 29, 28, 33], the Lode parameter value
32   might have an effect on fracture locus of the material. On the other hand, the referenced studies seems to indicate
33   that the effect of Lode parameter on the fracture is high at the low value of triaxiality and low at the high triaxiality
34   state for structural steels. The effect of Lode parameter was not studied in this paper and based on authors'
35   knowledge, it has not been studied for the materials used in the current research. Thus, a study concerning the
36   Lode parameter effect should be conducted in order to investigate it´s effect in the case of fracture near the weld
37   interface.

38   ## 6. Conclusions

39   In this research, the behavior and properties of round specimens subjected to tensile loading with and without
40   metallurgical constraints were studied. Based on the conducted experiments, measurements and FE analyses, the
41   following conclusions can be drawn:

42   1. Using notched tensile test specimens and the optimization routine, reliable material parameters can be
43   obtained for different steel grades.
44   2. The ultimate tensile strength increases but ductility decreases in the soft zone due to the metallurgical
45   constraint effect generated by the adjacent zones of higher hardness.
46   3. The Johnson-Cook material model can be used in the assessment of fractures in specimens with
47   metallurgical constraints.
48   4. The created material model can estimate the two different fracture initiation locations observed in the
49   experimental tests conducted for specimens with metallurgical constraints.

5. Value of the Lode parameter near the weld interface at CDB material is not constant. The model used in the study does not take into account the effect of Lode parameter. The effect of Lode parameter on the fracture in specimen with metallurgical constraints should be studied in more detail.

Acknowledgements

Funding

Data availability
The raw/processed data required to reproduce these findings cannot be shared at this time as they also form part of an ongoing study.

Use of the Quasi-Static Johnson-Cook Model in the Failure
Assessment of Tensile Specimens With Metallurgical Constraints
Riku Neuvonen, Tuomas Skriko, Timo Björk

31.3.2020

1 References

2

[1] C. Ouchi, "Development of steel plates by intensive use of TMCP and direct quenching processes," *ISIJ International,* vol. 41, no. 6, pp. 542-553, 2001.

[2] N. C. Muckelroy, K. O. Findley and R. L. Bodnar, "Microstructure and mechanical properties of direct quenched versus conventional reaustenitized and quenched plate," *Journal of Materials Engineering and Performance,* vol. 22, no. 2, pp. 512-522, 2013.

[3] J. Kömi, P. Karjalainen and D. Porter, "Direct-quenched structural steels," in *Encyclopedia of Iron, Steel and Their Alloys*, CRC Press, 2015.

[4] W.-S. Chang, "Microstructure and mechanical properties of 780 MPa high strength steels produced by direct-quenching and tempering process," *Journal of Material Science,* vol. 37, no. 10, pp. 1973-1979, 2002.

[5] A. H. Meysami, R. Ghasemzadeh, H. S. Seyedein and M. R. Aboutalebi, "An investigation on the microstructure and mechanical properties of direct-quenched and tempered AISI 4140 steel," *Materials & Design,* vol. 31, no. 3, pp. 1570-1575, 2010.

[6] D. A. Porter, "Weldable High-Strength Steels: Challenges and Engineering Applications," in *IIW International Conference High-Strength Materials - Challenges and Applications*, Helsinki, 2015.

[7] M. Amraei, T. Skriko, T. Björk and X.-L. Zhao, "Plastic strain characteristics of butt-welded ultra-high strength steel (UHSS)," *Thin–Walled Structures,* vol. 109, pp. 227-241, 2016.

[8] M.-M. Ran, F.-F. Sun, G.-Q. Li, A. Kanvinde, Y.-B. Wang and R. Y. Xiao, "Experimental study on the behavior of mismatched butt welded joints of high strength steel," *Journal of Constructional Steel Research,* no. 153, pp. 196-208, 2019.

[9] F.-F. Sun, M.-M. Ran, G.-Q. Li, Y.-B. Wang and R. Y. Xiao, "Strength model for mismatched butt welded joints of high strength steel," *Journal of Constructional Steel Research,* no. 150, pp. 514-527, 2018.

[10] D. M. Rodrigues, L. F. Menezes, A. Loureiro and J. V. Fernandes, "Numerical study of the plastic behaviour in tension of welds in high strength steels," *International Journal of Plasticity,* no. 20, pp. 1-18, 2004.

[11] T. Björk, A. Ahola and N. Tuominen, "On the design of fillet welds made of ultra-high-strength steel," *Welding in the World,* no. 62, pp. 985-998, 2018.

[12] T. Skriko, Dependence on Manufacturing Parameters on the Performance Quality of Welded Joints Made of Direct Quenched Ultra-High.Strength Steel, Lappeenranta: Acta Universitatis Lappeenrantaensis, 2018.

[13] G. Magudeeswaran, V. Balasubramanian and G. Madhusudhan Reddy, "Hydrogen induced cold cracking studies on armour grade high strength, quenched and tempered steel weldments," *Elsevier,* vol. 33, no. 7, pp. 1897-1908, 2008.

[14] G. R. Johnson and W. H. Cook, "A constitutive model and data for metal subjected to large strains, high strain rates and high temperatures," *Proceedings of the 7th International Symposium on Ballistics,* vol. 21, pp. 514-547, 1983.

[15] G. R. Johnson and W. H. Cook, "Fracture characteristics of three metals subjected to various strains, strains rates, temperatures and pressures," *Engineering Fracture Mechanics,* vol. 21, pp. 31-48, 1985.

[16] M. Nilsson, "Constitutive model for Armox 500T and Armox 600T at low and medium strain rates," FOI Swedish Defence Research Agency, 2003.

[17] M. A. Iqbal, K. Senthil, P. Sharma and N. K. Gupta, "An investigation of the constitutive behavior of Armox 500T steel and armor piercing incendiary projectile material," *International Journal of Impact Engineering,* vol. 96, pp. 146-164, 2016.

[18] J. Trajkovski, R. Kunc, V. Pepel and I. Prebil, "Flow and fracture behavior of high-strength armor steel PROTAC 500," *Materials & Design (1980-2015),* vol. 66 Part A, pp. 37-45, 2015.

[19] R. Bobbili, V. Madhu and A. K. Gogia, "Neural network modeling to evaluate the dynamic flow stress of high strength armor steels under high strain rate compression," *Defence Technology,* vol. 10, no. 4, pp. 334-342, 2014.

Use of the Quasi-Static Johnson-Cook Model in the Failure
Assessment of Tensile Specimens With Metallurgical Constraints
Riku Neuvonen, Tuomas Skriko, Timo Björk

31.3.2020

[20] N. Kılıç and B. Ekici, "Ballistic resistance of high hardness armor steels against 7.62 mm armor piercing ammunition," *Materials & Design,* vol. 44, pp. 35-48, 2013.

[21] N. Kılıç , S. Bedir, A. Erdik , B. Ekici , A. Taşdemirci and M. Güden, "Ballistic behavior of high hardness perforated armor plates against 7.62 mm armor piercing projectile," *Materials & Design,* vol. 63, pp. 427-438, 2014.

[22] M. A. Iqbal, K. Semthil, P. Bhargava and N. K. Gupta, "The characterization and ballistic evaluation of mild steel," *The characterization and ballistic evaluation of mild steel,* vol. 78, pp. 98-113, 2015.

[23] U. Zerbst, R. A. Ainsworth, H. T. Beier, H. Pisarski, Z. L. Zhang, K. Nikbin, T. Nitsche-Pagel, S. Münstermann, P. Kucharczyk and D. Klingbeil, "Review on fracture and crack propagationin weldments – A fracture mechanics perspective," *Engineering Fracture Mechanics,* no. 132, pp. 200-276, 2014.

[24] T. Børvik, O. S. Hopperstad, T. Berstad and M. Langseth, "A computational model of viscoplasticity and ductile damage for impact and penetration," *European Journal of Mechanics - A/Solids,* vol. 20, no. 5, pp. 685-712, 2001.

[25] A. Banerjee, S. Dhar, S. Acharyya, D. Datta and N. Nayak, "Determination of Johnson cook material and failure model constants and numerical modelling of Charpy impact test of armour steel," *Materials Science and Engineering: A,* vol. 640, pp. 200-209, 2015.

[26] A. A. Alabi, P. L. Moore, L. C. Wrobel, J. C. Campbell and W. He, "Tensile behaviour of S690QL and S960QL under high strain rate," *Journal of Constructional Steel Research,* vol. 150, pp. 570-580, 2018.

[27] K. Danas and P. P. Castaneda, "Influence of the Lode parameter and the stress triaxiality on the failure of elasto-plastic porous materials," *International Journal of Solids and Structures,* vol. 49, no. 11-12, pp. 1325-1342, 2012.

[28] K. S. Zhang, J. B. Bai and D. François, "Numerical analysis of the influence of the Lode parameter on void growth," *Dominique,* vol. 38, no. 23-33, pp. 5847-5856, 2001.

[29] M. Bruenig, S. Gerke and V. Hagenbrock, "Micro-mechanical studies on the effect of the stress triaxiality and the Lode parameter on ductile damage," *International Journal of Plasticity,* vol. 50, pp. 49-65, 2013.

[30] P. W. Bridgman, Studies in Large Plastic Flow and Fracture, Massachusetts: Harvard University Press, 1952.

[31] M. Alves and N. Jones, "Influence of hydrostatic stress on failure of axisymmetric notched specimens," *Journal of the Mechanics and Physics of Solids,* vol. 47, no. 3, pp. 643-667, 1999.

[32] Y. Bao, "Dependence of ductile crack formation in tensile tests on stress triaxiality, stress and strain ratios," *Engineering Fracture Mechanics,* vol. 72, no. 4, pp. 505-522, 2005.

[33] R. Kiran and K. Khandelwal, "A triaxiality and Lode parameter dependent ductile fracture criterion," *Engineering Fracture Mechanics,* vol. 128, pp. 121-138, 2014.

1

2